IEEE Access
Multidisciplinary | Rapid Review | Open Access Journal

Received November 7, 2016, accepted November 15, 2016, date of publication November 18, 2016,
date of current version December 8, 2016.

Digital Object Identifier 10.1109/ACCESS.2016.2630498

Closed Form Analysis of the Normalized Matched Filter With a Test Case for Detection of Underwater Acoustic Signals

ROEE DIAMANT
Department of Marine Technology, University of Haifa, Haifa 3498838, Israel
Corresponding author: R. Diamant (roeed@univ.haifa.ac.il)

ABSTRACT In this paper, closed-form expressions for the performance of the normalized matched filter (NMF) detector are developed specifically for the case of large time-bandwidth product, N. As a test case, the task of detecting underwater acoustic signals is considered. While the matched filter is the most common detector used, the NMF detector is used in cases where the ambient noise is fast time varying and is hard to estimate. While the performance of the NMF has been studied, no closed-form expressions are given for the detection and false alarm probabilities, and the accuracy of the available approximations greatly deteriorates with N. As a result, evaluating the detection threshold from the receiver operating characteristic requires significant, and sometimes untraceable, numerical calculations. This is specifically important for underwater acoustic signals, where due to the low signal-to-noise ratio, N is very large. The analysis performed in this paper solves this problem. The analysis is based on the probability distribution of the NMF to give an exact closed-form (tabulized) expression for the false alarm probability, and a relatively accurate approximation for the probability of detection, both for the large N case. These approximations are found accurate in numerical simulations. Results from an experiment conducted in the Mediterranean sea at the depth of roughly 1000 m validate the analysis.

INDEX TERMS Underwater acoustics, matched filter, detection, detection probability, false alarm probability, receiver operating characteristic.

I. INTRODUCTION

Underwater acoustics can fulfil the needs of a multitude of underwater applications. This include: oceanographic data collection, warning systems for natural disasters (e.g., seismic and tsunami monitoring), ecological applications (e.g., pollution, water quality and biological monitoring), military underwater surveillance, assisted navigation, industrial applications (offshore exploration), to name just a few [1]. To combat the low signal-to-noise ratio (SNR), underwater acoustic signals are characterized by a large time-bandwidth product, N. There detection is performed for a buffer of samples, $y(t)$, recorded from the channel (usually in a sliding time window fashion). In this paper, the focus is on detection of signals of known structure. The applications in mind are active sonar systems, acoustic localization systems (e.g., ultra-short baseline), and acoustic systems used for depth estimation, ranging, detection of objects, and communications.

We focus on the first step in the detection chain, namely, a binary hypothesis problem where the decoder differentiate between a *noise-only* hypothesis and a *signal exists* hypothesis. The former is when the sample buffer, $y(t)$, consists of ambient noise, and the latter is the case where the sample buffer also includes a distinct received underwater acoustic signal. Without prior information of the channel impulse response and noise (channel state information), the receiver must assume an additive white Gaussian noise (AWGN) channel. For such a channel, the most common detection scheme is the matched filter [2], which is optimal in terms of the SNR. The matched filter detector is a constant false alarm rate (CFAR) test, and its detection threshold is determined only by the target false alarm probability (cf. [6]). Due to the (possibly) large dynamic range of the detected signal [7], and for reasons of template matching [8], the matched filter is often normalized by the noise covariance matrix. This normalization is often referred to as normalized matched filter (NMF) and is the preferred choice in several tracking applications such as gradient descent search, active contour models, and wavelet convolution [9].

While the NMF has been analyzed before (e.g., in [10]), no closed form solutions are given for the false alarm and detection probabilities. The available expressions are still manageable for small N values. However, when N is large (say beyond 20), calculating these analytic expressions poses a significant computational burden. This is because, to select the detection threshold, one must draw the receiver operating characteristic (ROC) curve which shows the detection probability vs. the false alarm probability for different choices of the threshold. Hence, the calculation of the ROC must be efficient, preferably via closed form expressions. This problem is specifically important for underwater acoustic systems, where due to low signal-to-noise ratio and the existence of narrow band interferences, signals have a large time-bandwidth product with typical values of $N > 50$ [11]–[13]. Due to large time variation of the ambient noise, the NMF is widely used in underwater systems, and thus the efficient evaluation of the NMF ROC is specifically important for underwater acoustic applications. In this paper, we consider this need. For the NMF detector, we offer a closed-form analytical expression for the probability of false-alarm, and a relatively accurate approximation for the probability of detection. The developed expressions allow the immediate evaluation of the ROC. As a consequence, the performance of the NMF can be analyzed efficiently for different detector parameters. To summarize, the contribution of this work is twofold:

1) Providing closed form expressions for the detection and false alarm rate of the NMF detector in the large N limit.
2) A practical tool to set the detection threshold of the NMF detector in the large N limit.

Simulation results show that the developed expressions are accurate in the large N limit. To test the correctness of the analysis in real environment, results from a sea experiment are reported. The experiment was conducted in the Mediterranean sea to detect chirp signals reflected from the sea bottom at depth of roughly 1000 m.

The reminder of this paper is organized as follows. The system model is presented in Section III. In Section IV, we derive the probability distribution of the NMF and give expressions for the probability of false alarm and for the probability of detection. Next, performance evaluation in numerical simulation (Section V-A) and results from the sea experiment (Section VI-A) are presented in Section VI. Finally, conclusions are drawn in Section VII. The notations used in this paper are summarized in Table 1.

TABLE 1. List of major notations.

Notation	Explanation
$y(t)$	Received data from the channel
$s(t), s_k$	transmitted signal and its kth sample, respectively
$n(t), n_k$	Channel ambient noise and its kth sample, respectively
σ^2	variance of channel ambient noise
T	duration of signal
W	Bandwidth of signal
N	product of bandwidth and duration of signal
NMF	output of normalised matched filter
$x = \cos(\theta_{N-2})$	Output of NMF for $y(t) = n(t)$
$x_T = \cos(\theta_T)$	Detection threshold
$\cos(\phi)$	Output of NMF for $y(t) = s(t) + n(t)$
$P_{\rm FA}$	probability of false alarm
$P_{\rm D}$	probability of detection

II. BACKGROUND

In this work, the main assumption is that the receiver is aware of the structure of the transmitted signal, for which detection is usually based on the matched filter (MF) [14]. To serve as a detector, knowledge of the noise covariance is required, and as a result, several noise-only training signals are required [15]. Alternatively, based on the noise texture model, [16] suggested a maximum likelihood estimator for the noise covariance matrix. In [17], an iterative procedure is performed where first the covariance matrix is assumed known and the test statistics for a signal vector is calculated. Next, using these statistics and additional noise-only vectors, the noise covariance matrix is estimated and is substituted back into the test statistics. In [18], an adaptive matched subspace detector is developed and its statistical behavior is analyzed to adapt the detector to unknown noise covariance matrices in cases where the received signal is distorted compared to transmitted one. However, in fast time-varying environments such as in underwater acoustics [2], the estimated noise covariance is likely to be mismatched [19]. As shown in [20], mismatch in this estimation affects detection performance and target false alarm and detection rates may not be satisfied.

The MF detector requires knowledge of the noise variance. Hence, while the MF is the common detector when the structure of the signal is known, it cannot be properly used when the noise characteristics are fast time varying and hard to estimate. An alternative detection scheme is to normalize the matched filter with the power of the transmitted signal [2], [21]. The NMF detector does not require estimation of the noise covariance matrix. Instead, its detection threshold depends only on the time-bandwidth product, N, of the expected signal. This is because the normalization term cancels the noise contribution in the moments of NMF. The NMF is an appealing detector in cases where the noise is fast time varying. However, in the presence of multipath or noise transients, detection via the NMF degrades. Still, since the receiver is likely not to have prior knowledge of the channel, the NMF is widely used and was even patented [4].

An initial evaluation of the performance of the NMF detector is given in [22]. Based on the NMF eigenvalues, a more advanced analysis for radar detection is given in [23]. In [10], an NMF is suggested, where the linear matched filter is normalized by the power of the transmitted signal and a projection of the detected one. The projection is made according to the estimated noise covariance matrix, and the result is a simplified test which is proportional to the output of the standard colored-noise matched filter. A modification of the matched filter is proposed in [7] for the case of a multipath channel. The works in [7] and [10] include analysis for the false alarm and detection probabilities of the NMF.

However, this analysis is either a modification of a similar study of the NMF or is based on semi-analytic matrix representation. As such, it cannot provide means to evaluate closed form expressions to the performance of NMF. Alternatively, instead of deriving the distribution of the NMF, in [24], the NMF is appriximated by the Low Rank Normalized Matched Filter whose distribution is known, and a similar analysis with the adaptive matched filter is given in [25]. A distribution analysis of the NMF is given in [26]; And a bootstrap approximation is given for the NMF in [28]. However, the accuracy of this approximation fits signals with a small N value.

Some of the above works provide analytic expressions for the performance of the detector. These expressions are provided in non-closed terms (e.g., in [10]). While for signals of small N, which is suitable for most radio frequency applications, numerically evaluating these expressions is doable, for large N the calculation is not traceable. The work closest to the approach presented here was reported in [11], where for underwater acoustic communication, closed form expressions where provided for the false alarm and detection probability of the NMF detector. However, only approximated analysis is performed using orthonormal basis functions, whose accuracy reduce with N.

III. SYSTEM MODEL

In this work, the target application is detection of underwater acoustic signals. The underwater acoustic channel is a frequency selective channel with a long delay spread and complex ambient noise. However, since this channel is also fast time varying and space dependent, at the initial phase of signal detection the receiver cannot be assumed to know the channel or its charactaristics. Under these circumstances, for setting up the detection threshold the receiver must assume a simplified model. For a received signal, $y(t)$, we consider a binary detection test of hypotheses,

$$\begin{aligned} H_0 &: y(t) = n(t), \\ H_1 &: y(t) = s(t) + n(t). \end{aligned} \tag{1}$$

In (1), $s(t)$ is an underwater acoustic signal of bandwidth W, duration T, and $n(t)$ is an additive noise. Let us define the time-bandwidth product $N = WT$. We forbid oversampling, and thus N is also the number of time samples when sampling $y(t)$. We assume that N is large (values exceeding 50 are enough). As we show further below, the analysis made for the simplified model (1) agrees with experimental results. Without prior knowledge of the channel, we therefore argue that this model is a valid compromize.

We are interested in the following quantity (referred to as the NMF),

$$\begin{aligned} \text{NMF} &= \frac{\int s(t)y(t)dt}{\sqrt{\int s^2(t)dt \int y^2(t)dt}} \\ &= \frac{\sum_{k=1}^{N} s_k y_k}{\sqrt{\sum_k s_k^2 \sum_l y_l^2}}, \end{aligned} \tag{2}$$

where s_k and y_k are the kth sample of $s(t)$ and $y(t)$, respectively, and $y(t)$ is sampled regularly at the Nyquist rate. For a detection scheme which uses correlator (2) as its detection metric, the objective is to develop closed form expressions for the probability of false alarm and for the probability of detection, thereby allowing an immediate calculation of the ROC to choose the detection threshold for different system parameters. We note there is a considerable difference between the NMF in (2) and the regular matched filter. Specifically, the former includes a non-additive noise term that makes its analysis highly complicated and very different than for the latter (cf. [3]).

We consider the case of underwater acoustic signals, where the NMF in (2) operates on signals of large N. The underwater acoustic channel is a highly complex channel of long delay spread, many multipath, and non-stationary ambient noise with narrowband interference and noise transients. While, clearly, the channel affects the NMF's output, we assume a simplified model of an additive i.i.d Gaussian noise $n(t)$. This is because since the detector is performed at the very beginning of the detection process, the channel or its characteristics can not be assumed known. Thus, in the absence of prior knowledge of the channel impulse response and the distribution of the ambient noise, the detector has no choice but to set its detection threshold based on the above simplified assumption. Naturally, a mismatch in this model may lead to performance degradation. However, as we show in Section V-A for simulations and in Section VI-A, the effect on performance is not significant. Yet, the special case of coloured noise can be accounted for by including a trivial whitening mechanism in the filtering process. In this case, (2) becomes,

$$\frac{\sum_{j,k}^{N} s_j w_{j,k} y_k}{\sqrt{\sum_{j,k} s_j w_{j,k} s_k \sum_{j',k'} y_{j'} w_{j',k'} y_{k'}}}, \tag{3}$$

where w is the inverse correlation-matrix satisfying $\sum_k w_{j,k} E[n_k, n_l] = \delta_{j,k}$ and δ is the Kronecker delta function. The above whitening filter is performed prior to detection. Hence, the following results can therefore be generalized without the need of significant modifications.

Besides the noise model, another underline assumption in (3) is that $y(t)$ is of duration equal to that of the signal $s(t)$, and that in case of hypothesis H_1, it includes the transmitted signal in full. That is, the detector is time synchronized with the transmitter. In the case of underwater acoustics, this assumption is hard due to clock offsets, unknown propagation delay, and lack of coordination with the transmitter. Considering this, we suggest a fine-resolution detection process in which the NMF is processed over a sliding window block from the channel whose duration is larger than the signal transmitted. Then, instead of comparing a single NMF's output sample to the detection threshold, the detector compares the maximum of the NMF's output performed over the

processed block. This way, at the cost of complexity, no time synchronization is required for the detection process. It is noted that such processing is not a disadvantage per-se of the NMF. This is because a similar operation is required to any non-synchronized detector.

IV. PROBABILITY DISTRIBUTION ANALYSIS

In this section, we formulate the probability distribution of the NMF and for large N, give approximations for the probability of false alarm and for the probability of detection. To avoid the division with the norm of the transmitted and received signal, analysis is performed in spherical coordinates. For this reason, while usually the NMF is performed in complex baseband, the case of real $y(t)$ hat is easier to handle in spherical coordinates is considered. As will be discussed further below, the analysis performed for real signals also applies to complex ones. The difference between the NMF for complex and real signals lies in replacing the summations in (2) with an inner product while using the conjugate of the reference signal $s(t)$. Clearly, this operation does not change the moments of the NMF, and hence the following analysis for real signals also applies to complex signals with no need for adjustment.

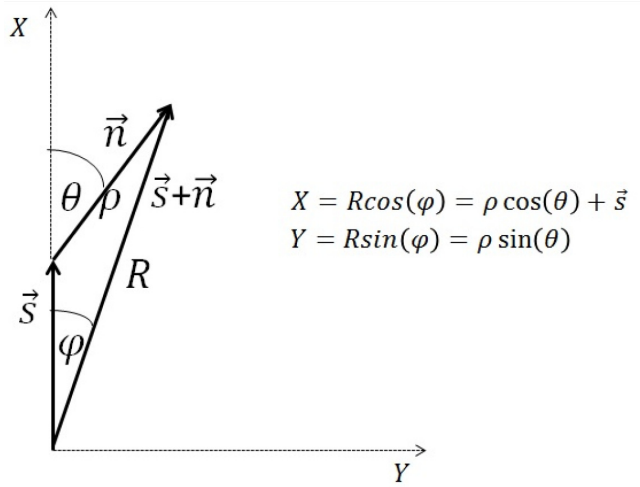

FIGURE 1. Spherical coordinates of received signal $s(t)$ and noise $n(t)$.

A. PROBABILITY OF FALSE ALARM

Let $\vec{s}$, $\vec{n}$ be N-dimensional space vectors whose elements are s_k and n_k, respectively. It is easier to manage the following analysis using spherical coordinates. To this end, we set $\vec{s}$ along the polar-axis (see Fig. 1), such that $\rho^2 = \sum_k n_k^2$. The assumption of i.i.d Gaussian noise leads to the probability density function

$$P(\rho, \phi, \theta_1, \ldots, \theta_{N-2})\, \partial\rho\partial\phi \prod_{k=1}^{N-2} \partial\theta_k = \left(2\pi\sigma^2\right)^{-\frac{N}{2}} e^{-\frac{1}{2\sigma^2}\sum_i n_i^2} \prod_l \partial n_l. \quad (4)$$

Then, for a noise-only signal, i.e., $y(t) = n(t)$, the NMF is given by the angle θ_{N-2} between vectors $\vec{s}$ and $\vec{n}$, such that

$$\text{NMF} = \frac{\vec{s}\cdot\vec{n}}{|\vec{s}||\vec{n}|} = \cos\theta_{N-2}. \quad (5)$$

To find the probability of false alarm, we first need to evaluate the distribution $P(\theta_{N-2})$. Then, given a detection threshold x_T, we obtain

$$\hat{P}_{\text{fa}} = \int_0^{x_T} P(\theta_{N-2}) d\theta_{N-2}. \quad (6)$$

Let the volume-element, $dV = \prod_l \partial n_l$, be expressed in terms of the solid angle $d\Omega$. Then, the volume element for $0 \le \phi \le 2\pi, 0 \le \theta_k \le \pi$ becomes

$$\begin{aligned} dV &= \rho^{N-1} d\rho d\Omega \\ &= \rho^{N-1}\partial\rho\partial\phi \prod_{k=1}^{N-2} \partial\theta_k \sin^k(\theta_k). \end{aligned} \quad (7)$$

Then, by integrating (4) over all angular variables, except for the polar-angle θ_{N-2}, one immediately obtains

$$P(\rho, \theta_{N-2}) \approx C_{N,1}\rho^{N-1} e^{-\frac{\rho^2}{2\sigma^2}} \sin^{N-2}(\theta_{N-2}), \quad 0 \le \theta_{N-2} \le \pi, \quad 0 \le \rho < \infty, \quad (8)$$

where $C_{N,1}$ is a constant. Further integration over ρ leads to

$$P(\theta_{N-2}) = C_{N,2} \sin^{N-2}(\theta_{N-2}), \quad (9)$$

and $C_{N,2}$ is a constant. For convenience, denote $x = \cos(\theta_{N-2})$. Expression (9) implies that all the odd moments of x vanish identically, whereas even moments are given by

$$E\left[x^{2p}\right] = \frac{\Gamma\left(\frac{N}{2}\right)}{\sqrt{(\pi)}} \frac{\Gamma\left(p+\frac{1}{2}\right)}{\Gamma\left(p+\frac{N}{2}\right)}, \; p = 0, 1, 2, \ldots. \quad (10)$$

In particular,

$$E\left[x^2\right] = \frac{1}{N}. \quad (11)$$

The result in (11) can be obtained directly by the method described in the Appendix, which confirms the above analysis.

By (9) and (11), when $N >> 1$ the distribution $P(\theta_{N-2})$ approaches the Gaussian limit with the variance being $\frac{1}{N}$. Then, the probability of false alarm is approximated by

$$\hat{P}_{\text{fa}} = \frac{1}{2}\text{erfc}\left(x_T\sqrt{\frac{N}{2}}\right), \quad (12)$$

However, since usually $P_{\text{fa}} << 1$, unless N is huge such that $P_{\text{fa}}N >> 1$ expression (12) is not accurate enough. Instead, the accurate term for the probability of false alarm is

$$P_{\text{fa}} = 1 - B\left(x_T^2, \frac{1}{2}, \frac{N-1}{2}\right), \quad (13)$$

where

$$B(a,b,z)=\int_0^a t^{b-1}(1-t)^{z-1}dt$$

denotes the (tabulated) regularized incomplete beta function.

Note that (13) does not require calculation of the noise characteristics. This allows an easy calculation of the detection threshold even before performing detection. Consider for example a target false alarm probability of 10^{-4}. For $N = \{20, 30, 50, 100\}$, the threshold becomes $\{0.75, 0.63, 0.5, 0.36\}$. Similarly, for $P_{\text{fa}} = 10^{-3}$, for $N = \{20, 30, 50, 100\}$, the threshold becomes $\{0.65, 0.53, 0.42, 0.3\}$.

B. PROBABILITY OF DETECTION

1) EXACT TERM

Suppose $y(t) = s(t) + n(t)$, and mark s^2 as the energy of the received signal. Setting $\vec{s}$ along the polar-axis (see Fig. 1) we have $\vec{y}\cdot\vec{s} = R\cos(\phi)$ with NMF $= \cos(\phi)$. Therefore, changing variables (ρ, θ_{N-2}) into (R, ϕ) in (8) we obtain

$$P(R,\phi)\approx R^{N-1}\sin^{N-2}(\phi)e^{-\frac{(R\cos(\phi)-s)^2+R^2\sin^2(\phi)}{2\sigma^2}},$$
$$-\le\phi\le\pi, 0\le R<\infty. \tag{14}$$

Integrating over R, $P(\phi)$ can be written in terms of the parabolic-cylinder function,

$$D_p(z)=\frac{1}{\pi}\int_0^\pi \sin(p\alpha)-z\sin(\alpha))\,d\alpha,$$

i.e.,

$$P(\phi)=\pi^{-\frac{1}{2}}2^{1-\frac{N}{2}}\frac{\Gamma(N)}{\gamma\left(\frac{N-1}{2}\right)}e^{-s^2\frac{\frac{1}{2}-\frac{1}{4}\cos^2(\phi)}{\sigma^2}}\sin^{N-2}(\phi)$$
$$\cdot D_N\left(-s\frac{\cos(\phi)}{\sigma}\right). \tag{15}$$

Alternatively, by the definition of $D_p(z)$,

$$P(\phi)=\frac{e^{-\frac{s^2}{2\sigma^2}}\sin^{N-2}(\phi)}{\sqrt{\pi}\Gamma\left(\frac{N-1}{2}\right)}\cdot\left[\Gamma\left(\frac{N}{2}\right)F\left(\frac{N}{2},\frac{1}{2},\frac{s^2\cos^2(\phi)}{2\sigma^2}\right)\right.$$
$$\left.+\Gamma\left(\frac{N+1}{2}\right)\sqrt{2}s\frac{\cos(\phi)}{\sigma}F\left(\frac{N+1}{2},\frac{3}{2},\frac{s^2\cos^2(\phi)}{2\sigma^2}\right)\right], \tag{16}$$

where

$$F(a,b,z)=\frac{\Gamma(b)}{\Gamma(b-a)\Gamma(a)}\int_0^1 e^{zt}t^{a-1}(1-t)^{b-a-1}dt$$

is the confluent hypergeometric function. Denote the SNR $\rho = \frac{s}{\sigma}$. Note that as $\rho \to 0$, (16) is reduced back to (9).

The average NMF, derived from (16), is given by the Kummer function,

$$E[\cos(\phi)]=\frac{\Gamma\left(\frac{N+1}{2}\right)}{\Gamma\left(\frac{N+2}{2}\right)}\frac{se^{-\frac{s^2}{2\sigma^2}}}{\sqrt{2\sigma^2}}F\left(\frac{N+1}{2},\frac{N+2}{2},\frac{s^2}{2\sigma^2}\right). \tag{17}$$

The probability of detection for the detection threshold, x_T, can be found by

$$P_D=\int_0^{x_T}P(\phi)d\phi. \tag{18}$$

Similar expressions as in (18) can be found in the literature to evaluate the detection probability of the NMF detector (cf. [7], [10]). These expressions can be evaluated numerically when N is small to calculate the detection probability almost exactly. However, for large N direct numerical calculation of P_D is bound to fail. This is because $P(\phi)$ contains infinitely many terms which oscillate rapidly as $N \gg 1$. Unfortunately, this is he case in underwater acoustic signals. It is therefore important to obtain asymptotic expressions for $P(\phi)$ in the large-N limit.

2) APPROXIMATED SOLUTION

When both N and ρ are large compared to unity, $P(\phi)$ can be approximated using the asymptotic form of $D_p(z)$ [29],

$$D_p(z)\approx e^{-\frac{z^2}{4}}z^p\left(1+\mathcal{O}\left(\frac{z}{p}\right)\right), \tag{19}$$

applicable for $z >> 1$ and $|z| >> |p|$ (i.e., for large SNR). However, this may not be applicable to all considered cases. Instead, the *correct* asymptotic can be found by expanding $P(\phi)$ around its saddle-point.

To that end, let us go back to expression (14). Denoting $R \to \tilde{R}\frac{\sqrt{N}}{\sigma}$, and introducing $\gamma = \frac{s}{2\sigma\sqrt{N}}$, (14) takes the form

$$P_\gamma(\tilde{R},\phi)\approx\left(\tilde{R}\sin^2(\phi)\right)^{-1}e^{Ng}, \tag{20}$$

where $g = \ln(\tilde{R}) + \ln(\sin(\phi)) - \frac{1}{2}\tilde{R}^2 + 2\tilde{R}\gamma\cos(\phi)$. Note that γ is a function of ρ (which corresponds to the SNR). Since $P_\gamma = 0$ at the end points $(\tilde{R}, \phi) = (0, 0)$ and $(\tilde{R}, \phi) = (\infty, \pi)$, the large-$N$ behaviour of this function is dominated by Gaussian fluctuations around some saddle-points in the complex $(\tilde{R} \times \phi)$-hyper plane. The saddle-points equations are then

$$\frac{\partial g}{\partial\tilde{R}}=\tilde{R}^{-1}-\tilde{R}+2\gamma\cos(\phi)=0,$$
$$\frac{\partial g}{\partial\phi}=\cot(\phi)-2\tilde{R}\gamma\sin(\phi)=0, \tag{21}$$

with fluctuations determined by the following Hessian (also known by the name ''Fisher information

matrix'')

$$H = \begin{pmatrix} \frac{\partial^2 g}{\partial \tilde{R}^2} & \frac{\partial^2 g}{\partial \tilde{R}\partial\phi} \\ \frac{\partial^2 g}{\partial\phi\partial\tilde{R}} & \frac{\partial^2 g}{\partial\phi^2} \end{pmatrix} = -\begin{pmatrix} \tilde{R}^{-2}+1 & 2\gamma\sin(\phi) \\ 2\gamma\sin(\phi) & 2\tilde{R}\gamma\cos(\phi+\frac{cos(\phi)}{\sin^2(\phi)}) \end{pmatrix}. \quad (22)$$

Equation (21) is solved by the quartet

$$R_c = \frac{2\gamma^2 \pm \sqrt{4\gamma^4+4\gamma^2+1}}{\sqrt{4\gamma^2+1}}, \quad (23)$$

$$\sin(\phi_c) = \pm\frac{1}{\sqrt{4\gamma^2+1}}. \quad (24)$$

Fortunately, only one of these solutions (the one for which $R_c, \phi_c \geq 0$) is reachable by a continuous deformation of the contour of integration. Substituting back into (22), one obtains

$$|g''| = -\frac{\partial^2 g}{\partial\phi_c^2} = 1+4\gamma^2+\frac{4\gamma^4}{1+4\gamma^2}\left(2\gamma^2+\sqrt{4\gamma^4+4\gamma^2+1}\right). \quad (25)$$

To the leading order in powers of N^{-1} and for arbitrary values of $\gamma \geq 0$,

$$P_\gamma(\phi) \approx \sqrt{\frac{N|g''|}{2\pi}} e^{-\frac{N}{2}|g''|(\phi-\phi_c)^2}, \quad N >> 1. \quad (26)$$

For $\gamma << 1$ (i.e., small SNR), we get $\phi_c \approx \left(\frac{\pi}{2}-2\gamma\right)$ and $|g''| \approx 1$. Therefore, (26) implies that the NMF maintains good deflection as long as $\gamma N > 1$, which is similar to other compressing filters. (Note that under this condition, the variance of ϕ is smaller than the SNR separation). In the opposite limit, as γ increases, $\phi_c \approx 2\gamma^{-1}$ approaches towards the edge-point $\phi = 0$. At the same time, however, $|g''| \to 4\gamma^4$ and $\frac{\mathrm{var}(\phi)}{\phi_c^2} \approx \frac{N\gamma^2}{-1} << 1$. Thus, when $\phi_c \to 0$, the Gaussian lube shrinks thereby avoiding any significant deformations due to edge-effects. As a result the probability of detection, P_d, can be evaluated as

$$P_D = \frac{1}{2}\mathrm{erfc}\left((\phi_c-\theta_T)\sqrt{\frac{N|g''|}{2}}\right), \quad \phi_c < \theta_T < \frac{\pi}{2}. \quad (27)$$

This approximation introduces a relative error of the order $\mathcal{O}\left(N^{-1}\right)$ in the estimation of P_D. It follows from (27) that, for a fixed ρ, as the number of samples N is increased, P_d is saturated.

The above analysis provided an exact closed form expression (12) for the false alarm probability, and a closed form approximation for the detection probability (27). These expressions can be readily used to obtain the ROC. Having expressions (12), (25), and (27), one can construct the ROC in the large-N limit. First, the detection threshold is obtained by inverting (12). Next, $|g''|$ is calculated with the help of (27). Finally, the required ρ ratio is determined by solving (25) for γ. The above process is demonstrated in Fig. 2, where we show the obtained ROC curves for $N = 100$ for different SNR values. Due to the closed form expressions (12) and (27), the ROC was obtained with no computational burden.

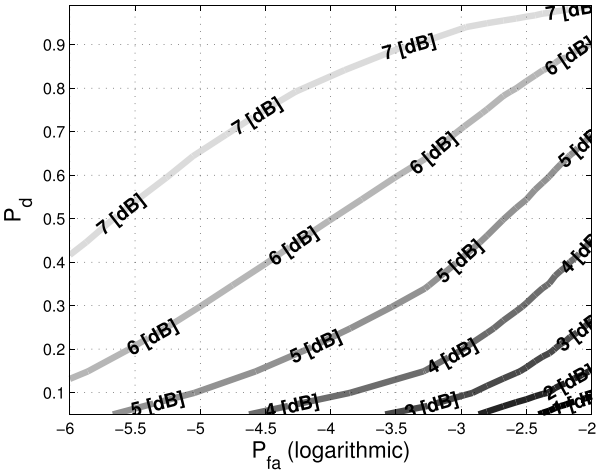

FIGURE 2. ROC curves for $N = 100$. Contour lines represents SNR values ρ. Logarithm base 10.

V. PERFORMANCE EVALUATION

To evaluate the accuracy of the expressions for P_{fa} and P_D, results from numerical simulations and from a sea experiment are now presented. To that end, the above analysis is compared with empirical measurements of the probability of false alarm, $\hat{P}_{\mathrm{fa}}$, and the probability of detection, $\hat{P}_D$. This is performed by counting the number of occurrences for which NMF $> \cos(\theta_T)$ when $y(t) = n(t)$ and when $y(t) = s(t) + n(t)$, respectively. Unless stated otherwise, we determine the detection threshold based on a target $P_{\mathrm{fa}} = 10^{-4}$, i.e., a CFAR detector. For efficiency, the sample buffer $y(t)$ and the reference signal $s(t)$ are downscaled baseband converted. As mentioned above, no adjustment is needed in the analysis due to the transformation from the case of real signals to the case of complex ones.

As stated in Section III, the assumed model of i.i.d Gaussian noise likely does not realistic underwater acoustic channels, and a mismatch in performance is foreseen. Still, with no prior knowledge of the channel, this simplified channel model is the best practice. To show the effect of setting the detection threshold based on this simplified model, along side verifying the exact term in (12) and the approximation in (27) for the channel considered in the system model, it is of interest to test how significant the effect of this mismatch is. To that end, in this section the accuracy of the develop expressions are shown also for the case of non Gaussian noise, and for the case of a realistic channel collected during a sea experiment. The results will show that no significant performance degrade exists.

A. SIMULATIONS

The numerical simulations include transmission of a linear frequency modulation (LFM) chirp signal. The duration of the signal is set for $T_s = 50$ msec, and its bandwidth varies with the considered N. Compliant with the system model, an AWGN channel is assumed. The effect of the channel on performance is shown for the sea experiment discussed further below. As a benchmark, comparison is performed with the analysis in [11] for the NMF. While in this work the false alarm probability is derived exactly, the term for the false alarm in [11] is approximated. Hence, the latter is used as a benchmark only for the case of detection, since both in [11] and in this work the detection probability of the NMF is approximated for underwater acoustic signals with large N. Comparison between the expression in (27) and the benchmark was made for a fixed threshold of 0.17 and as a function of the signal-to-noise ratio. For completeness, the detection probability benchmark approximation from [11] is quoted here:

$$P_D^{\mathrm{BM}} \approx Q\left(\frac{\mathrm{Th}-\mu}{\epsilon}\right), \tag{28}$$

where μ and ϵ are the mean and variance of the NMF output, set for an AWGN channel with no Doppler scale.

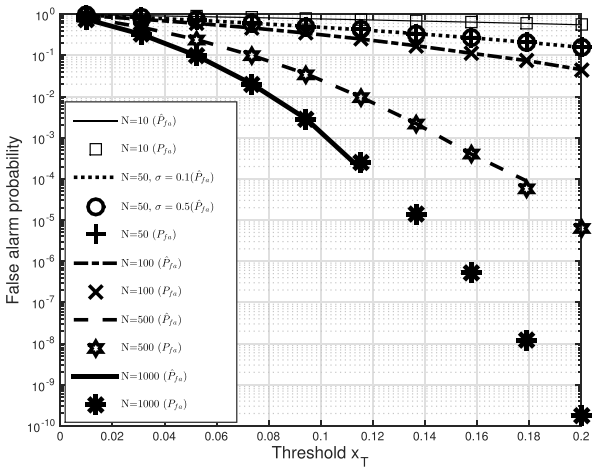

FIGURE 3. Probability of false alarm as a function of detection threshold.

In Fig. 3, results for the probability of false alarm are shown for a white Gaussian noise. Good match between the analysis (p_{fa}) and the empirical ($\hat{p}_{fa}$) results is observed. The results show the strong dependency between threshold θ_T from (12) and the compression ratio N. That is, for the same target probability of false alarm the threshold level dramatically decreases as N increases. Fig. 3 also shows results of $\hat{P}_{\mathrm{fa}}$ for two ρ ratios. As expected, the probability of false alarm does not depend on the SNR, i.e., the NMF detector is indeed a CFAR test.

In Fig. 4, approximation (27) is verified for several compression ratios N for a white Gaussian noise. Analysis p_d and the empirical $\hat{p}_d$ results are given. Results are shown as a function of ρ. One can observe that P_D increases with N.

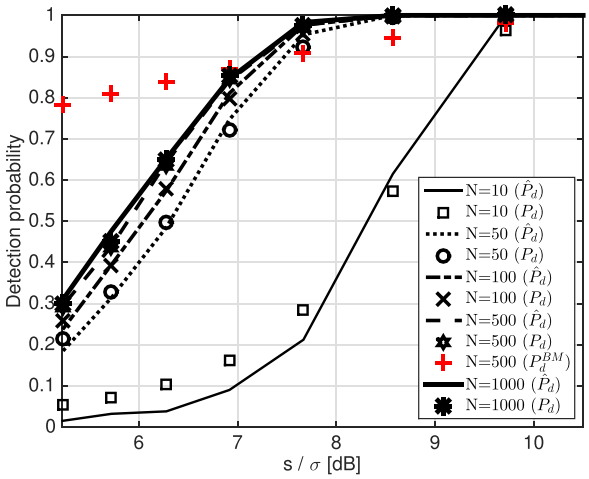

FIGURE 4. Probability of detection as a function of ρ. Performance are compared with the analysis in [11]. Target $P_{\mathrm{fa}} = 10^{-4}$.

This is because of the dependency of threshold x_T in N. However, for high levels of N, P_D saturates. Fig. 4 shows that for small values of N, there is only a rough match between the analytic approximation P_D and the empirical measurement $\hat{P}_D$. This is due to the use of the saddle-point approximation in (21), which applies for large N. Therefore, in the small N limit, a better approach would be to numerically evaluate other available expressions (e.g., [7]) that for small N are still traceable. However, from Fig. 4 one can see that for higher values of N and starting from $N = 50$, a sufficient match is observed with no numerical analysis. This result clarify why this work is limited for signals of large N. Fig. 4 also shows the comparison between the benchmark approximated detection probability and the term in (27). The results show that the term in (27) is significantly more accurate then the benchmark analysis. We note that a similar gap in the accuracy of the evaluation is obtained also for other N values. This is because unlike in [11] where for calculating the detection probability the NMF is approximated as a Gaussian, in (27) the Gaussian approximation is considered only around the saddle-point.

Next, we test how setting the detection threshold based on our analysis fits also the case of a more complex noise. We consider two realistic noise components: a strong single carrier interference at the centre frequency (*CW*) that simulates the effect of interference formed by e.g., eco-sounders, and a sea noise recorded during a sea experiment (*Exp noise*). An example of an Exp noise is shown in Fig. 5a, and the empiric pdf evaluated for all noise instances used is shown in Figure 5b. One can observe the strong random transients in the experiment noise resulting wideband interferences, and the noise pdf appears to be similar to a Laplace Gaussian. For the case of CW, we explore the results for a noise term combining both i.i.d. Gaussian noise and a CW. In all cases, the detection threshold is set according to (13), i.e., only for Gaussian noise. For each case, we perform 10^5 Monte-Carlo simulation runs. For the case of CW, in each run only the i.i.d.

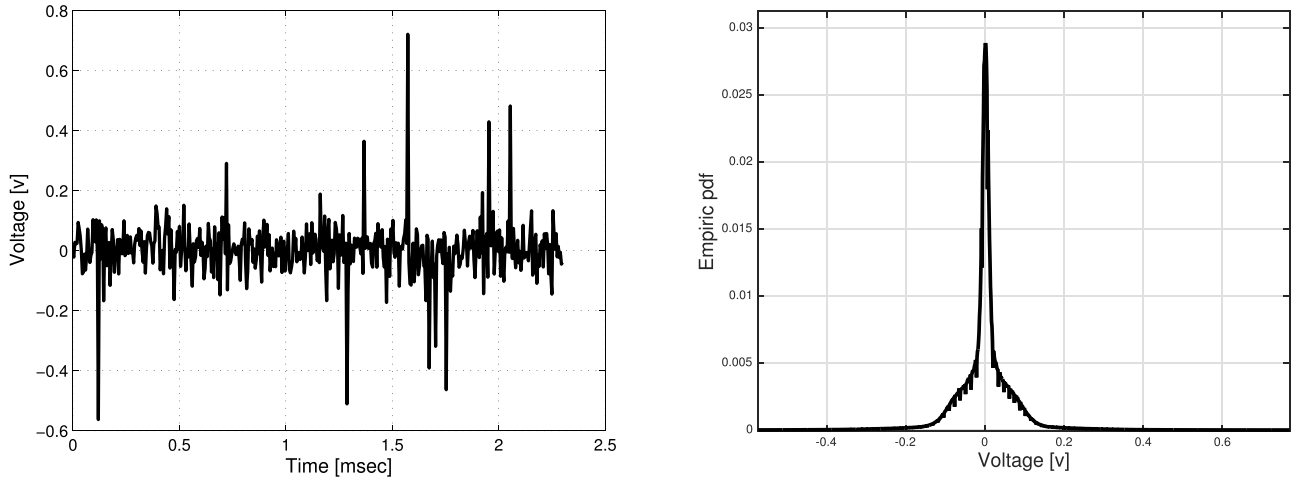

(a) (b)

FIGURE 5. Recorded noise from sea experiment: (a) a single time-domain example, (b) empirical PDF.

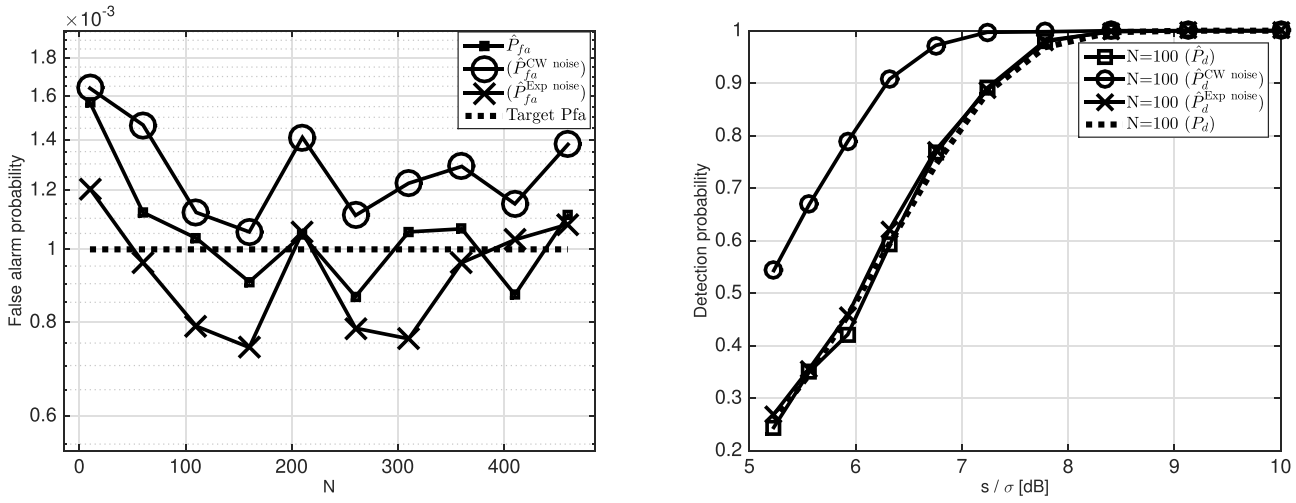

(a) (b)

FIGURE 6. The effect of mismatch in noise model on the detector performance: (a) Probability of false alarm as a function of N for target $P_{\text{fa}} = 10^{-3}$ (b) Probability of detection as a function of ρ for target $P_{\text{fa}} = 10^{-4}$.

Gaussian noise is randomized, while for the Exp noise case in each run we use different instances of recorded noise. In case of the CW interference, the power of the CW is made equal to that of the i.i.d Gaussian term. To explore the effect of the complex noise terms on the detection rate, for all three cases we alter the energy of the noise components to fit different SNR values.

Fig. 6a shows results for the probability of false alarm, where $\hat{p}_{fa}$ represents results for i.i.d. Gaussian noise only, $\hat{p}_{fa}^{\text{CW noise}}$ represents results for i.i.d. Gaussian noise with a CW interference, $\hat{p}_{fa}^{\text{Exp noise}}$ represents results for Exp noise, and the target false alarm probability is set for $p_{fa} = 10^{-3}$. Performance are shown for different N values. Clearly, since the detection threshold is determined while considering only an i.i.d Gaussian noise term, we expect differences in the results for the above three noise cases. However, Fig. 3 shows that $\hat{p}_{fa}$, $\hat{p}_{fa}^{\text{CW noise}}$, and $\hat{p}_{fa}^{\text{Exp noise}}$ are on the same order. Compliant with the results from Fig. 3, this match exists for both small and large values of N. That is, in terms of false alarm, the analysis holds also for complex noise terms. The performance in terms of the detection rate is shown in Fig. 6b. Here, we set the detection threshold for a target false alarm of 10^{-4}. Small differences are observed between our analytic approximation, p_d, the simulated case of i.i.d Gaussian noise only, $\hat{p}_d$, and the case of Exp noise, $\hat{p}_d^{\text{Exp noise}}$. However, much better detection rates than the expected ones are observed for the case of Gaussian noise with CW, $\hat{p}_d^{\text{CW noise}}$. The reason is that while the CW is considered in the calculation of the SNR (with equal power to the i.i.d Gaussian noise term), since the transmitted signal is wideband, the contribution of the narrowband CW interference greatly decreases after the NMF. We therefore conclude that both in terms of false

alarm rate and detection rate, the analysis made can be used also for detection of signals in complex environments.

VI. PERFORMANCE EVALUATION

The results from the simulations verify the correctness of (12). Furthermore, for underwater acoustic signals where the common case is $N > 50$, approximation (27) predicts the probability of detection and thus the ROC. In addition, the results show that the analysis holds for an ambient noise consisting a single carrier interference and for the realistic case of noise recordings from a sea experiment.

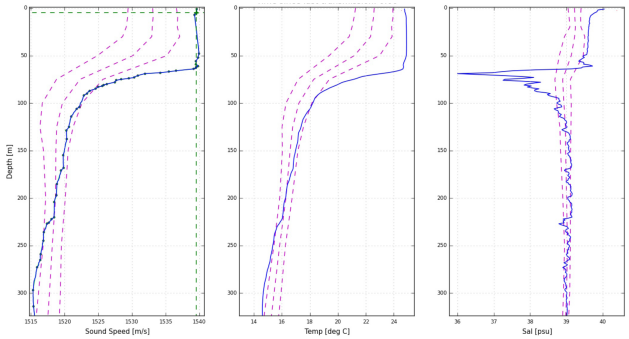

FIGURE 7. Sound speed profile, temperature, and salinity. Measured during the sea experiment.

A. SEA EXPERIMENT

Since, at the phase of signal detection, the receiver cannot assume to have channel state information, the analysis in this paper is made for an additive white Gaussian noise (AWGN) channel. To show the practicability of the analysis (12) and (27) and to test its robustness to realistic channels, we now explore its validity in real environments. The experiment took place in August 2014, and was performed 10 km off the shores of Haifa, Israel, at water depth of roughly 1000 m. The sound speed profile, temperature, and salinity, measured at the upper layer of the water column is shown in Fig. 7. We observe a strong thermocline around 60 m. The experimental setup included a surface vessel from which a transmitting projector and a receiving hydrophones were deployed. The transmitter was located at water depth of 50 m, and the hydrophone was placed at water depth of 100 m. The transmitter-receiver range was roughly 50 m. The experiment included 600 underwater acoustic transmissions. Each transmission consisted of two linear frequency modulation chirp signals, spaced by a time gap of 100 msec, whose carrier frequency was 50 kHz, bandwidth 10 kHz, and whose duration varied between: 10msec, 50msec, and 100msec. The tested N values were therefore 100, 500, and 1000. Several ρ values were tested by changing the amplification level of the transmitted signals. Transmissions were made at depth of 10 m, and signals were received at depth of 100 m. This depth difference allowed sufficient separation between the receptions of the direct path, surface reflections, and bottom reflections, while allowing the use of a narrow voltage range to reduce quantization errors.

TABLE 2. Results from sea experiment.

N	ρ [dB]	Measured Detection Rate	Prob. of Detection (analysis)
100	≤ 0	0/57 (0)	0.0022
	5	3/17 (0.17)	0.21
	10	29/32 (0.9)	1
	15	26/26 (1)	1
	$\geq$20	68/68 (1)	1
$\geq$500	$\leq$0	1/51 (0.01)	0.0021
	5	5/22 (0.22)	0.235
	10	35/38 (0.92)	1
	15	37/37 (1)	1
	$\geq$20	52/52 (1)	1

Following each transmission, a sampled buffer of 2 sec was collected from the channel. A time-frequency response of one of these sample buffers is shown in Fig. 8a. The dominant templates of the two transmitted chirps observed around time instances 4.1 s and 4.2 s are related to the direct path from the transmitter and to surface reflections. Considering that the transmitter-bottom-receiver path length was roughly 1850 m and assuming the average sound speed was roughly as shown in Fig. 8b, the weaker templates observed around time instances 5.3 s and 5.4 s are related to reflections of the two chirps from the sea bottom. The received signals included strong multipath arrivals. An example to such multipath is observed in Fig. 8b, where we show the output of the NMF for the latest arrival. Since the transmitted signal was wideband, the output of the NMF can serve as a rough estimate of the channel's impulse response [27]. Hence, considering the time delay between the first and last significant peaks in Fig. 8b, we conclude that the impulse response length was roughly 20 ms (or 30 m). For each detected signal, the SNR ρ was evaluated by estimating the arrival time of the received signal and measuring the signal energy and the noise level.

Detection of the two chirp signals was performed using the NMF detector with target $P_{\text{fa}} = 10^{-4}$ and detection threshold (12). Accurate detection was verified by comparing the time difference of arrival of each two local maxima of the NMF response with the expected time gap between the two transmitted chirp signals (100 msec). On the other hand, miss detection was declared when the output of the NMF did not exceed threshold. False alarm was determined for cases when the NMF response exceeded the threshold at wrong timing.

The decoding of the sea experiment achieved no false alarm. Considering the time window used for the sample buffer, this outcome corresponds to zero false alarms for roughly 2500 trials. The results for the detection rates are given in Table 2 alongside the predicted approximation (27). Since for high values of N the probability of detection changes little with N (see Fig. 4), results for $N \geq 500$ are accumulated. In addition, for clarify, the measured ρ levels are quantized. Compliant with the analysis, no miss detection was found at ρ levels above 15 dB. However, for lower ρ ratios, detection performances are a bit below the expected level. This is explained by the effect of the

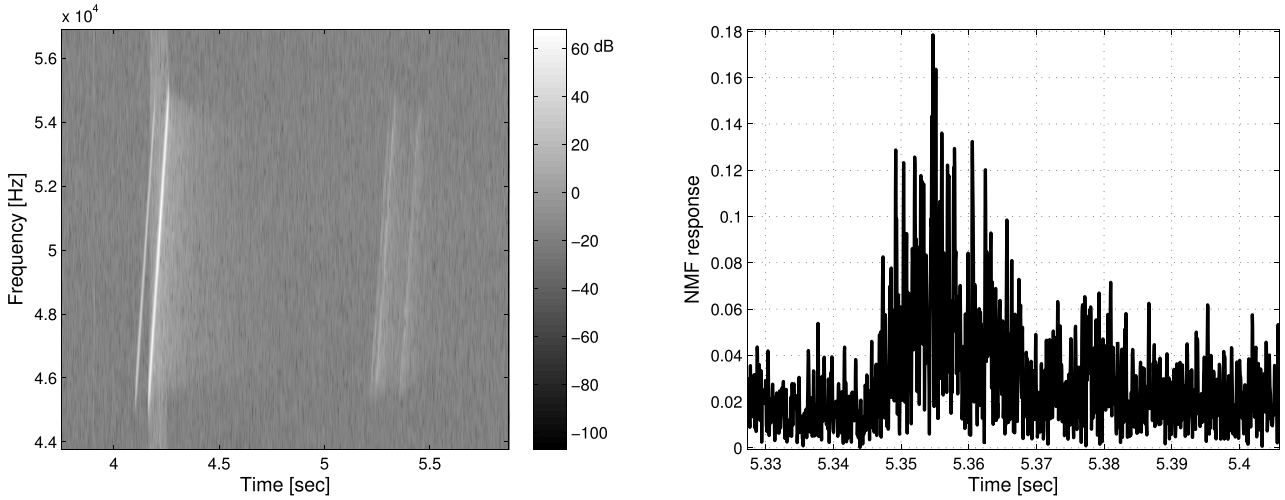

FIGURE 8. Buffer recorded during the sea experiment (depth roughly 1000 m): (a) Time-frequency response, (b) Output of the NMF for the latest arrival.

non-linear channel (especially the Doppler shift phenomena and non-resolved multipath) on performance, which distorts the received signal and thus reduces the output of the NMF. Nonetheless, considering the fact that the detection probability fast increases with the SNR (see Figs. 4 and 6b) and that the measured detection rates are collected within an SNR range of 5 dB, the differences shown in Table 2 are rather small. We therefore argue that the analysis in this work can serve as a good indicator for the performance in a real sea environment.

VII. CONCLUSIONS

This paper focused on the performance of the normalized matched filter (NMF). The NMF is used when the noise covariance matrix is fast time-varying and is hard to estimate. While the performance of the NMF has been studied, no closed expressions are given for the false alarm and detection probabilities. As a result, calculating the ROC for large time-bandwidth product N requires a significant, and sometime non-traceable, numerical calculation effort. As a result, it maybe hard to set the detection threshold for different system parameters. This specifically affects underwater acoustic applications where, due to the low signal-to-noise ratio, N is large. Considering this problem, this work provided closed form expressions for the false alarm and detection probabilities, and thus an immediate method to calculate the ROC and choose the detection threshold. The analysis involved derivation of the probability distribution and the moments of the NMF. Then, both the exact finite-N distribution (16) and the large-N limit (26) were studied. For the case of large N value, exact expression for the probability of false-alarm (12) and an approximation for the probability of detection (27) were developed. Numerical simulations showed that the developed expressions are accurate. Results of a sea experiment shows small differences between the measured detection rate and the analysis for the detection probability.

APPENDIX

VIII. SECOND MOMENT OF A NMF

In this section expression for the second moment of the NMF (2) are developed for the case of $y(t) = n(t)$. For a sampled noise signal with a sampling period Δ and number of samples N,

$$\mathrm{NMF}^2 = \frac{\left(\sum_{k=1}^{N} n_k s_k \Delta\right)^2}{\left(\sum_{k=1}^{N} n_k^2 \Delta\right) \cdot \left(\sum_{k=1}^{N} s_k^2 \Delta\right)}. \tag{29}$$

Denote $\tilde{n}_k = \frac{n_k}{\sigma}$, $\tilde{s}_k = s_k \sqrt{\frac{\Delta}{E_s}}$, where σ^2 is the variance of $n(t)$ and E_s is the energy of $s(t)$. Then,

$$\mathrm{NMF}^2 = \frac{\left(\sum_{k=1}^{N} \tilde{n}_k \tilde{s}_k \Delta\right)^2 \sigma^2 \frac{E_s}{\Delta}}{\left(\sum_{k=1}^{N} \tilde{n}_k^2 \Delta\right) \cdot \left(\sum_{k=1}^{N} \tilde{s}_k^2 \Delta\right) \sigma^2 \frac{E}{\Delta}}. \tag{30}$$

Clearly, $E\left[\mathrm{NMF}^2\right]$ does not depend on σ or E_s. In the following, s_k and n_k are therefore refer to as normalized variables. The second moment of the sampled NMF is

$$E\left[\mathrm{NMF}^2\right] = E\left[\frac{\sum_{k,l}^{N} s_k s_l \cdot n_k n_l}{\left(\sum_{m=1}^{N} n_m^2\right)}\right]. \tag{31}$$

To simplify (31), one can use the connection

$$\frac{1}{X} = \int_0^\infty e^{-\lambda X} d\lambda, \tag{32}$$

such that

$$E\left[\mathrm{NMF}^2\right] = \sum_{k,l}^{N} s_k s_l \cdot E\left[\int_0^\infty n_k n_l e^{-\lambda \sum_m n_m^2} d\lambda\right]. \tag{33}$$

Since n_k is Gaussian, so is the integral in (33) and

$$E\left[\mathrm{NMF}^2\right] = \sum_k^N s_k^2 \cdot E\left[\int_0^\infty n_k^2 e^{-\lambda \sum_m n_m^2} d\lambda\right]. \quad (34)$$

Consider $N = 1$. Here,

$$E\left[\mathrm{NMF}^2\right] = \int_{-\infty}^{\infty} \frac{dn}{\sqrt{2\pi}} \int_0^\infty n^2 e^{-n^2\left(\lambda+\frac{1}{2}\right)} d\lambda$$
$$= \frac{\Gamma\left(\frac{3}{2}\right)}{\sqrt{2\pi}} \int_{\frac{1}{2}}^\infty \frac{da}{a^{\frac{3}{2}}} = 1, \quad (35)$$

where $a2$ is used. The result in (35) is a good sanity check since for the case of a single sample, the variance of the NMF is 1. For a general N,

$$E\left[\mathrm{NMF}^2\right] = \sum_k s_k^2 \cdot \frac{1}{(2\pi)^{\frac{N}{2}}} \Gamma\left(\frac{3}{2}\right) \pi^{\frac{N-1}{2}} \int_{\frac{1}{2}}^\infty \frac{da}{a^{\frac{3}{2}} a^{\frac{N-1}{2}}}$$
$$= \frac{\sqrt{\pi}}{2^{\frac{N}{2}}} \cdot \frac{1}{N} \pi^{-\frac{1}{2}} 2^{\frac{N}{2}} = \frac{1}{N}. \quad (36)$$

By (36), the variance of NMF for the case of noise-only signal is inverse proportional to N.

REFERENCES

[1] I. Akyildiz, D. Pompili, and T. Melodia, "State-of-the-art in protocol research for underwater acoustic sensor networks," in *Proc. ACM Int. Workshop Underwater Netw. (WUWNet)*, Sep. 2006, pp. 7–16. [Online]. Available: http://dx.doi.org/10.1145/1161039.1161043

[2] W. Burdic, *Underwater Acoustic System Analysis*, 2nd ed. Englewood Cliffs, NJ, USA: Prentice-Hall, 2002.

[3] S. M. Kay, *Fundamentals of Statistical Signal Processing: Detection Theory*, vol. 2, A. V. Oppenheim, Ed. Englewood Cliffs, NJ, USA: Prentice-Hall, 1998.

[4] D. W. Davis, J. H. Michels and J. R. Román, "Normalized parametric adaptive matched filter receiver," U.S. Patent 6 771 723, Aug. 3, 2004.

[5] S. M. Kay, *Fundamentals of Statistical Signal Processing: Detection Theory*, vol. 2. Englewood Cliffs, NJ, USA: Prentice-Hall, 1998.

[6] D. Kazakos and P. Papantoni-Kazakos, *Detection and Estimation*, vol. 65. New York, NY, USA: Computer Science Press, 1990.

[7] G. Bumiller and L. Lampe, "Fast burst synchronization for power line communication systems," *EURASIP J. Adv. Signal Process.*, no. 1, p. 166, May 2007. [Online]. Available: http://dx.doi.org/10.1155/2007/12145

[8] E. Conte, M. Lops, and G. Ricci, "Adaptive detection schemes in compound-Gaussian clutter," *IEEE Trans. Aerosp. Electron. Syst.*, vol. 34, no. 4, pp. 1058–1069, Oct. 1998.

[9] J. Lewis, "Fast normalized cross-correlation," in *Proc. Vis. Interface*, vol. 10. 1995, pp. 120–123.

[10] M. Rangaswamy, "Normalized matched filter—A low rank approach," in *Proc. Conf. Rec. 36th Asilomar Conf. Signals, Syst. Comput.*, Nov. 2002, pp. 1267–1271. [Online]. Available: http:// dx.doi.org/10.1109/acssc.2002.1196984

[11] S. F. Mason, C. R. Berger, S. Zhou, and P. Willett, "Detection, synchronization, and Doppler scale estimation with multicarrier waveforms in underwater acoustic communication," *IEEE J. Sel. Areas Commun.*, vol. 26, no. 9, pp. 1638–1649, Dec. 2008.

[12] D. Rouseff, M. Badiey, and A. Song, "Effect of reflected and refracted signals on coherent underwater acoustic communication: Results from the Kauai experiment (KauaiEx 2003)," *J. Acoust. Soc. Amer.*, vol. 126, no. 5, pp. 2359–2366, 2009. [Online]. Available: http:// dx.doi.org/10.1121/1.3212925

[13] P. A. van Walree and R. Otnes, "Ultrawideband underwater acoustic communication channels," *IEEE J. Ocean. Eng.*, vol. 38, no. 4, pp. 678–688, Oct. 2013.

[14] D. Dardari, A. Conti, U. Ferner, A. Giorgetti, and M. Z. Win, "Ranging with ultrawide bandwidth signals in multipath environments," *Proc. IEEE*, vol. 97, no. 2, pp. 404–426, Feb. 2009.

[15] E. Kelly, "Performance of an adaptive detection algorithm; Rejection of unwanted signals," *IEEE Trans. Aerosp. Electron. Syst.*, vol. 25, no. 2, pp. 122–133, Mar. 1989. [Online]. Available: http://dx.doi.org/10.1109/7.18674

[16] A. Younsi and M. Nadhor, "Performance of the adaptive normalized matched filter detector in compound-Gaussian clutter with inverse gamma texture model," *Prog. Electromagn. Res. B*, vol. 32, pp. 21–38, Oct. 2011. [Online]. Available: http:// dx.doi.org/10.2528/pierb11051905

[17] F. C. Robey, D. R. Fuhrmann, E. J. Kelly, and R. Nitzberg, "A CFAR adaptive matched filter detector," *IEEE Trans. Aerosp. Electron. Syst.*, vol. 28, no. 1, pp. 208–216, Jan. 1992.

[18] S. Kraut, L. L. Scharf, and L. T. McWhorter, "Adaptive subspace detectors," *IEEE Trans. Signal Process.*, vol. 49, no. 1, pp. 1–16, Jan. 2001.

[19] D. A. Abraham and P. K. Willett, "Active sonar detection in shallow water using the page test," *IEEE J. Ocean. Eng.*, vol. 27, no. 1, pp. 35–46, Jan. 2002.

[20] L. Scharf and D. Lytle, "Signal detection in Gaussian noise of unknown level: An invariance application," *IEEE Trans. Inf. Theory*, vol. 17, no. 4, pp. 404–411, Jul. 1971.

[21] L. L. Scharf, S. Kraut, and M. L. McCloud, "A review of matched and adaptive subspace detectors," in *Proc. IEEE Adapt. Syst. Signal Process. Commun. Control Symp.*, Oct. 2000, pp. 82–86. [Online]. Available: http://dx.doi.org/10.1109/asspcc.2000.882451

[22] E. Conte, M. Lops, and G. Ricci, "Adaptive matched filter detection in spherically invariant noise," *IEEE Signal Process. Lett.*, vol. 3, no. 8, pp. 248–250, Aug. 1996.

[23] A. Kammoun, R. Couillet, F. Pascal, and M.-S. Alouini. (2015). "Optimal design of the adaptive normalized matched filter detector." [Online]. Available: https://arxiv.org/abs/1501.06027

[24] A. Combernoux, F. Pascal, G. Ginolhac, and M. Lesturgie, "Asymptotic performance of the low rank adaptive normalized matched filter in a large dimensional regime," in *Proc. IEEE Int. Conf. Acoust. Speech Signal Process. (ICASSP)*, Apr. 2015, pp. 2599–2603.

[25] A. D. Maio, "A new derivation of the adaptive matched filter," *IEEE Signal Process. Lett.*, vol. 11, no. 10, pp. 792–793, Oct. 2004.

[26] A. Younsi and M. Nadour, "Performance of the adaptive normalized matched filter detector in compound-Gaussian clutter with inverse gamma texture model," *Prog. Electromagn. Res. B*, vol. 32, pp. 21–38, Jun. 2011.

[27] R. Diamant and L. Chorev, "Emulation system for underwater acoustic channel," in *Proc. Int. Undersea Defence Technol. Eur. Conf. (UDT)*, Amsterdam, The Netherlands, vol. 1. Jun. 2005, pp. 2–6.

[28] W. Jing and J. Yong, "Bootstrap-based parametric adaptive matched filter detector: CFAR performance analysis," in *Proc. IEEE Int. Conf. Signal Process. Commun. Comput. (ICSPCC)*, Sep. 2015, pp. 1–5.

[29] I. Gradshteyn and I. Ryzhik, *Table of Integrals, Series, and Products*, 7th ed. San Diego, CA, USA: Academic, 2007.

ROEE DIAMANT received the Ph.D. degree from the Department of Electrical and Computer Engineering, The University of British Columbia, in 2013, and the B.Sc. and the M.Sc. degrees from the Technion - Israel Institute of Technology, in 2002 and 2007, respectively. From 2001 to 2009, he was with Rafael Advanced Defense Systems, Israel, as a Project Manager and System Engineer, where he developed a commercial underwater modem with network capabilities. From 2015 to 2016, he was a Visiting Professor with the University of Padua, Italy. He is currently leading the Underwater Acoustic And Navigation Laboratory, Department of Marine Technology, University of Haifa, as a Senior Lecturer (equivalent to Assistant Professor). In 2009, he received the Israel Excellent Worker First Place Award from the Israeli Presidential Institute, the NSERC Vanier Canada Graduate Scholarship in 2010, and two best paper awards. He serves as an Associate Editor of the IEEE Ocean Engineering. His research interests are in underwater acoustic communication, underwater navigation, object identification, and classification.